A classical molecular dynamics simulation method for the formation of “dry” gels from boro-aluminosilicate glass structures

Mélanie Taron, Jean-Marc Delaye, Stéphane Gin
CEA, DES, ISEC, DE2D, University of Montpellier, Marcoule, F-30207 Bagnols-sur-Cèze, France

Abstract

In contact with water, glass transforms into amorphous and porous structures called gels. A simulation method based on classical molecular dynamics is proposed here to mimic “dry” gels forming from initial oxide glass structures. Six glass compositions were investigated. Two behaviours were evidenced depending on the initial glass composition, and in particular on the quantity of elements removed. If a large quantity of soluble elements (B, Na) was removed, it induced an increase in the average pore size within the gels, and the time needed to stabilise the gel structure increased because more local atomic rearrangements occurred. The gel network displayed a higher proportion of Si-Q_4 at the expense of Si-Q_3 and a lower average ring size compared to the glass network, irrespective of the glass composition. Surface effects were also highlighted in the dry gels, such as the presence of 3-coordinated Al and a decrease in the average angle Si-O-Si and Al-O-Al. These findings will be compared to both wet gels and experimental data in further studies, to help find the best procedure to simulate such structures.

Introduction

Borosilicate glasses are of great technological interest because of their versatility and the various properties they offer[1]. One of their many applications is found in the nuclear field, where they are used to contain high-level radioactive wastes from spent nuclear fuel reprocessing. After cooling for a few decades, the vitrified wastes will be stored in a deep geological repository[2]. To prepare for this, many studies have been performed on glass durability in order to assess the safety of such a disposal system over a geological time scale[2-5]. It has been observed that when in contact with water, glass dissolves firstly at an initial rate, then decreasingly through time until it reaches a rate several orders of magnitude lower, called the residual rate[2]. This decrease has been attributed to the formation of a passivating alteration layer, usually referred to as gel[6,7].

The gel is characterised by its porous, amorphous, and hydrated structure. Depending on its open porosity, it can act as a diffusion barrier for aqueous species[8,9]. The mechanisms behind the formation of such a gel have been widely discussed, resulting in two main theories: the gel may be defined as a “residual” glass skeleton depleted in soluble elements such as alkali and boron[8,10], or on the other hand, it may be the result of the precipitation of dissolved species at the interface with the altering solution[11,12]. However, neither approach necessarily excludes the other.

To date, there no consensus has been reached as to the origin of the passivating effect of gels, which thus remains an open question. Studies have suggested that it may originate from their ability to act as a barrier to both water and reaction product diffusion, thus limiting the dissolution process by

partially sealing diffusive canals[13,14]. Another explanation, proposed by Du et al.[15], suggests an increase in the number of small silicate rings within the gels resulting in a decrease in water mobility.

However, it appears that the passivating properties of the gel greatly rely on several factors, such as the glass composition[14,16] and the altering solution composition (pH[17,18], concentration of ions[19-22]). Consequently, it is also important to underline that the morphology of the gel also changes over time due to a maturation process[23] and the incorporation of exogenous elements[20,21], making it even harder to ascribe the passivation to one definitive mechanism. Several studies have investigated gel morphologies. For example, it has been shown that the size of the pores depends on the pH of the solution, as higher pH levels lead to an increasing porosity due to the higher solubility of silicon[24]. Moreover, a gel morphology can display open and/or closed pores[13], as well as an uneven pore distribution through the gel layer, which can appear to be denser at the interface with the solution[24]. Many studies have been conducted on the impact of the glass composition on gel properties, by both experimental approaches and Monte-Carlo simulations[16,25-27]. While these have highlighted the role of specific elements such as Al[27], to date no global model has emerged to enable a better understanding of the link between glass composition and gel properties. In this study we focused on six glasses and gels of various compositions by classical molecular dynamics. This two-part study is attempting to link both the structure and the composition of gels to various properties of the passivating layer.

Classical molecular dynamics simulations have proven to be an invaluable tool in probing the structure of glasses[10,28-30] and gels[31,32] at both short and medium range order. Several methods exist to simulate gels, from the removal of blocks of silicon atoms to simulate an ordered porosity[33,34], to the introduction of defects using hydrogarnet defects[32] or modification of the simulation parameters, for example like charge scaling, mimicking a sol-gel process[35], and volume scaling[36,37]. However, it has not yet been possible to directly reproduce the experimental mechanisms leading to the formation of the gel with water. Classical molecular dynamics were therefore used here to study six simulated "dry" (without water) gels. The gels were obtained from five-oxide (Si-Al-B-Na-Ca) glasses and then depleted in soluble elements, with the exception of calcium which has already been proven to be retained in the gel layer[10,38]. The gels were annealed in order to simulate their stabilisation with time, enabling a continuous, dynamic structural analysis. Comparisons between the gels and their respective glasses will give an indication of the impact of the initial glass composition on the structure and morphology of the gel. This paper details the first part of a longer study intended to simulate wet gels by introducing water into the porous volumes of the dry gels described here. These wet gel properties will be presented in a second article.

Methods

Glass compositions

	Composition (mol%)					S/I	SiO_2/Al_2O_3	Density[39] (g/cm^3)	T (K)
	SiO_2	B_2O_3	Al_2O_3	CaO	Na_2O				
S65.5	65.50	9.00	6.84	6.00	12.66	0.3	9.6	2.49	3400
S57.5	57.50	18.00	5.84	6.00	12.66	0.6	9.8	2.44	3000
S51.0	51.00	22.00	5.34	6.00	12.66	0.9	9.6	2.34	3400
S52.5	52.50	19.00	9.84	6.00	12.66	0.6	5.3	2.36	3200
S57.5	57.50	18.00	5.84	6.00	12.66	0.6	9.8	2.44	3000

S63.0	63.00	17.00	1.34	6.00	12.66	0.6	47.0	2.48	3000
CJ3	61.16	16.29	3.89	5.81	12.85	0.6	15.7	2.47	3200

Table 1 – Composition, soluble / insoluble ratio (S/I), SiO_2 /Al_2O_3 ratio, density and maximum simulated temperature T of the studied glasses

Six five-oxide glasses divided into two series were designed in order to assess the impact of two particular ratios (the ratio between soluble and insoluble elements, S/I, and the SiO_2/Al_2O_3 ratio) on the structure and properties of the resulting simulated gels. The compositions are given in Table 1. In the first series, composed of S65.5, S57.5, and S51.0, the SiO_2/Al_2O_3 ratio remained constant with only the S/I ratio varying. Inversely, with a varying SiO_2/Al_2O_3 ratio and constant S/I ratio, the second series was composed of S52.5, S63.0, and S57.5, to which was added CJ3 which has been studied elsewhere and meets the necessary criteria[40].

In order to define the soluble and insoluble elements, the following assumptions were made based on previous studies, either by MD or experiments[10,38]:

- Soluble elements are B, Ca, and the quantity of Na associated with non-bridging oxygen (H1)
- Insoluble elements are Si and Al (H2)
- Four fold-coordinated Al^4 is compensated before four fold-coordinated B^4, and firstly by Na, then Ca (H3)
- B^4 is compensated by Na (H4).

For instance, using S52.5 as an example, the S/I calculation is as follows: from (H3), the Al quantity is inferior to the Na quantity, meaning that all Al are compensated by Na. From (H4) and (H3), the quantity of B compensated by Na is the remaining quantity of Na that does not compensate Al. The 4-fold coordinated B quantity is therefore (Na_2O_3 - Al_2O_3): all Na are charge compensators and there are no Na associated with non-bridging oxygens. Thus, from (H1), the soluble elements correspond to the Ca and B atoms, i.e. CaO + 2*B_2O_3. The insoluble elements are, from (H2), the quantity of Si and Al, i.e. SiO_2 + 2*Al_2O_3.

Simulation of the glasses

Glasses were prepared using the LAMMPS code[41] with potentials (Coulomb - Buckingham type) developed by Du et al[28] (see Supplementary Information Table S1 and Table S2) following Equation (1), taking into account two-body potentials at short range (a repulsive exponential term and an attractive dipolar term) and long-range Coulombic interactions:

$$V_{ij} = A_{ij}e^{-\frac{r_{ij}}{\rho_{ij}}} - \frac{C_{ij}}{{r_{ij}}^6} + \frac{q_i q_j}{r_{ij}} \quad (1)$$

where *i* and *j* are the atoms of the *i-j* pair, A_{ij}, ρ_{ij} and C_{ij} are the short range pair potential parameters, r_{ij} the interatomic distance between the atoms *i* and *j*, and q_i and q_j are the partial charges for the atoms *i* and *j*. A repulsive term described in Equation (2) was added to overcome strong attractions at small interatomic distances induced by the Buckingham potential:

$$V_{ij}(r_{ij}) = \frac{B_{ij}}{{r_{ij}}^{n_{ij}}} + D_{ij}{r_{ij}}^2 \quad (2)$$

where B_{ij}, n_{ij} and D_{ij} are parameters fitted to allow continuity in the potential, the force, and the first derivate of the force at the distance where the second derivate of the force is close to zero.

The simulated systems were composed of 100 000 randomly generated atoms, for which the box size was determined with respect to the estimated density of each glass based on Fluegel's work[39]. Long-range interactions were computed with a Particle-Particle-Particle-Mesh (PPPM) algorithm, with a defined accuracy of 10^{-5}. The cut-off used for the short-range interaction was 10 Å. All simulations

were performed with a 1 fs time step. A first equilibration step was performed at 1000 K for 0.1 ps in the NVT ensemble (constant number of atoms, volume, and temperature) to remove the initial most energetic interactions. The structure thus obtained was then heated to 3000 K < T < 3400 K for 1 ns (NVT ensemble) in order to lose the memory of the initial configuration, and quenched at a 2 K/ps rate to 300 K in the NVT ensemble. Afterward, two successive 20 ps equilibration steps were performed, firstly in the NVT ensemble, then in the NVE ensemble (constant number of atoms, volume, and energy).

Formation of the gels

Gels were obtained from the simulated glass by removing all boron atoms as well as all sodium, with the exception of two gels (S65.5 and S52.5). For these, part of the sodium was used to compensate aluminium and thus it was left in the gel. In order to maintain the electro-neutrality of the system, it was necessary to remove some oxygen atoms. They were selected randomly from the boron and sodium first-neighbour environments. Once prepared, the new system was equilibrated for 0.5 ns in the NVT at 300 K ensemble before being heated to 2400 K in the same conditions. This step was conducted for 0.5 ns, and enabled the gel structure to be annealed and stabilised. Tests were conducted to determine the heating temperature of the annealing and its effect on the porosity, and the results are displayed in Supplementary Information Figure S1. The relaxation temperature was chosen above 2000K to be in the second part of the curve (the part with the steeper slope) to ensure sufficient relaxation to obtain pores with radii of the order of the experimental ones (around 0.5nm). Overly hot temperatures were also avoided, to prevent the structures from melting with subsequent pore collapse. Finally an intermediate temperature of 2400K was selected. Afterwards the system was instantly cooled to 300 K, at which two successive NVT and NPT (isobaric) relaxations were performed for 20 ps each.

Analysis methods

King rings

Rings were calculated following the King's criterion, which states that a ring is considered the shortest path between a given atom and its nearest neighbours[42].

Pore size distribution (PSD)

To estimate the pore morphology and topology of the gels, the pore size distribution can be calculated using the method developed by Bhattacharya and Gubbins[43]. The pores are explored using a spherical probe of varying size in order to find the largest sphere fitting in the pore. The PSD is defined as the statistical distribution of the radii of these spheres.

Coordination number

The cut-off radii used to calculate the coordination numbers are given in Table 2. They correspond to the first minimum after the first peak of the radial distribution function.

	Si-O	B-O	Al-O	Na-O	Ca-O
r_{cut} (Å)	2.1	2.0	2.4	3.5	3.2

Table 2 – Cut-off radii used for the coordination number analysis

Surface atoms

To determine the quantity of surface atoms, a method based on the calculation of the local Voronoï volumes was used. For surface atoms located at the pore surface, the local Voronoï volume is larger than for bulk atoms. To identify surface atoms, 3 million points in the simulation box were chosen at random. The number of points nearest to a given atom than any other atoms was calculated for each atom of the system. Hence, the surface atoms can be identified because of a larger quantity of points

around them compared to the bulk atoms. A threshold was determined for each gel (Table 3). An atom is considered to be a surface atom if the number of points around it is superior to this threshold. Each threshold was determined empirically by verifying visually that it allowed a clear separation between the surface and the bulk atoms.

	S65.5	S63.0	CJ3	S52.5	S57.5	S51.0
Threshold	75	90	88	86	90	105

Table 3 – Threshold used to identify the surface atoms for each gel

Results

Structural comparison between simulated pristine glasses and alteration gels

Coordination number (CN)

		S65.5		S63.0		CJ3		S52.5		S57.5		S51.0	
		Glass	Gel	Glass	Gel	Glass	Gel	Glass	Gel	Glass	Gel	Glass	Gel
Mean CN	Si	4.00	4.00	4.00	3.99	4.00	4.00	4.00	4.00	4.00	4.00	4.00	3.99
	Al	4.01	3.81	4.02	3.67	4.01	3.67	4.01	3.88	4.01	3.70	4.01	3.67
	Ca	6.64	5.67	7.03	4.73	6.97	5.08	6.90	5.87	6.99	5.24	7.04	5.07
(%)	NBO	7.5	3.9	6.8	8.0	5.9	5.8	3.2	5.5	4.5	4.9	3.3	6.0
	O^2	91.4	93.9	92.6	91.8	93.0	93.2	93.7	90.6	93.8	93.1	94.9	92.0
	O^3	1.1	2.2	0.6	0.2	1.1	1.0	3.1	3.9	1.7	2.0	1.8	2.0
Q_n Si (%)	Q_4	81.2	91.2	82.9	83.6	84.8	87.6	90.8	86.6	87.7	89.0	90.4	86.3
	Q_3	17.8	8.6	16.3	15.8	14.6	12.0	9.0	12.9	11.9	10.6	9.4	13.2
	Q_2	1.0	0.2	0.8	0.6	0.6	0.4	0.2	0.5	0.4	0.4	0.2	0.5
	Q_1	0.0	0.0	0.0	0.0	0.0	0.0	0.0	0.0	0.0	0.0	0.0	0.0
	Q_0	0.0	0.0	0.0	0.0	0.0	0.0	0.0	0.0	0.0	0.0	0.0	0.0
Q_n Al^4 (%)	Q_4	97.3	97.9	98.0	97.0	98.0	97.5	98.8	97.0	98.7	97.3	99.0	97.2
	Q_3	2.7	2.0	1.9	3.0	2.0	2.5	1.2	3.0	1.3	2.7	1.0	2.8
	Q_2	0.0	0.1	0.1	0.0	0.0	0.0	0.0	0.0	0.0	0.0	0.0	0.0
	Q_1	0.0	0.0	0.0	0.0	0.0	0.0	0.0	0.0	0.0	0.0	0.0	0.0
	Q_0	0.0	0.0	0.0	0.0	0.0	0.0	0.0	0.0	0.0	0.0	0.0	0.0
Angles (°)	Si-O-Si	151.7	151.4	151.4	150.7	151.4	150.7	152.2	150.5	151.8	150.6	152.4	150.2
	O-Si-O	109.4	109.4	109.4	109.4	109.4	109.4	109.4	109.4	109.4	109.4	109.4	109.4
	O-Al-O	109.2	110.1	109.1	110.9	109.2	110.9	109.2	109.7	109.2	110.6	109.2	110.8
	Si-O-Al	144.1	142.5	143.6	143.6	143.5	143.2	144.3	141.3	143.9	142.0	144.6	141.6
	Al-O-Al	128.8	119.6	129.3	126.3	130.5	121.2	126.7	121.4	126.5	120.9	127.1	122.5
Mean free volume/pore radius (Å)		0.56	1.24	0.54	2.37	0.54	2.01	0.57	3.71	0.56	2.60	0.59	4.46
Mean ring size		5.60	5.25	5.70	5.18	5.66	5.19	5.60	5.11	5.64	5.16	5.78	5.10

Table 4 – Mean CN of Si, Al, and Ca, percentages of NBO, O^2, and O^3, Qn distribution of Si and Al, calculated mean angle, mean free volume/pore radii and mean ring size in the simulated initial pristine glass and the alteration gels

Table 4 displays the mean CN of Si, Al, and Ca for the glasses and their respective gels. The Si mean CN remains unchanged between glass and gel, which demonstrates the stability of the silicon tetrahedron in both glass and gel. However, it can be seen that both Al and Ca mean CN significantly decrease. For all the glasses, Al is found in tetrahedral form, consistent with experimental data on alumino-borosilicate glasses[10,44]. Its mean CN value decreases to between 3.88 and 3.67 in the gels,

which shows the presence of 3-fold coordinated Al. This drop is larger when the Al content decreases. A decrease between the Ca mean CN in the gel compared to the glass can also be seen (from a 6.64 – 7.04 range for the glasses to 4.73 - 5.87 for the gels). Non-bridging oxygens (NBO) and the 2 and 3-fold coordinated oxygen percentage are given in the second part of Table 4. Globally, they display only minor variations and no clear tendency can be deduced from the NBO % comparison between the glasses and the gels, but the NBO % mostly increase in the gels except for S65.5 and CJ3. Conversely, the O^2 % decreases in the gels compared to the glasses, with the same exception for S65.5 and CJ3. The O^3 % is less than 3%, except for S52.5. While the existence of these species has never been confirmed experimentally, several molecular dynamics studies have shown their existence in equilibrated glasses[45-47]. In our compositions, the O^3 % increases with the Al % content in the gels and a similar trend is observed for the glasses (except for S65.5 and S57.5), which could indicate that the O^3 entities play a role of charge compensator. The O^3 % increases in the gel compared to the glass, except for S63.0 and CJ3.

Additionally, Si and Al^4 Q_n species were calculated for glasses and gels alike (Table 4). It appears that the Si Q_4 percentage generally increases at the expense of Q_3 in the gels compared to their glasses, except for S52.5 and S51.0 for which the percentage decreases. These two glasses have the lowest SiO_2 percentages. S65.5 shows the greatest increase in Q_4, from 81.2% to 91.1%, which can be attributed to the low soluble/insoluble ratio and the higher Si percentage. Furthermore, the Si Q_4 percentage is higher than that observed experimentally[10]. It could be related to a faster reconstruction of the Si at the expense of the Al. Changes in the Q_n population relative to Al^4 appear to be negligible.

Angle

The mean angle values of different M-O-M or O-M-O (M = Si, Al) linkages in both glasses and gels can be found in Table 4. It appears that for all the gels, the Si-O-Si, Si-O-Al (except S63.0), and Al-O-Al angle values decrease, with a larger decrease for the latter. While the O-Si-O mean value remains constant, ranging from 109.36 to 109.60° (standard value for the tetrahedron angle), the O-Al-O angle slightly increases in the gels compared to the glasses. This can be explained by an increase in the Al^3 quantity, creating trihedra with internal angles close to 120°.

Rings

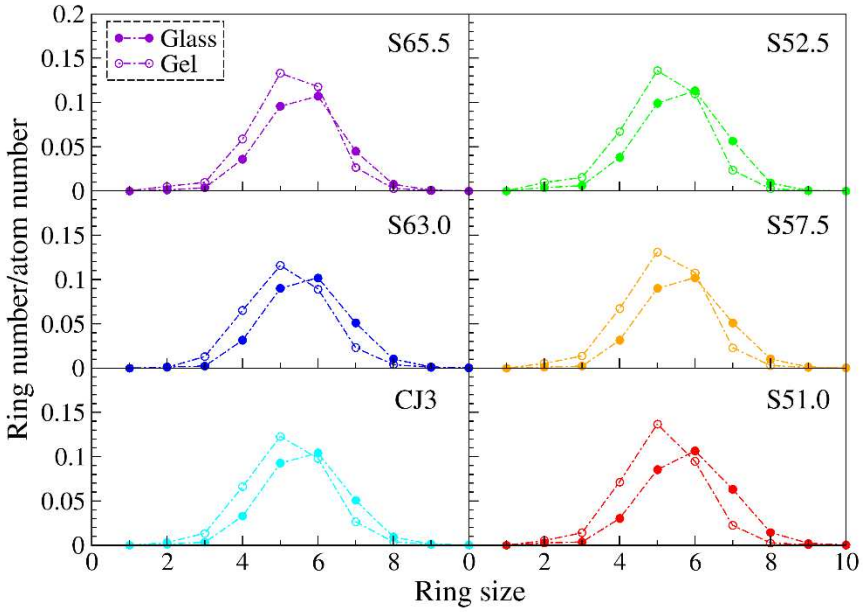

Figure 1 – Distributions of King ring sizes in the initial glasses and in the dry gels

Figure 1 shows the King ring size distribution[42] for both glasses and gels. It appears that in the glasses the maximum ring population is centred at a value of 6, while it is centred on 5 in the gels. The ratios of mean ring size between a gel and its parent glass were calculated. From these results, it can be seen that the glasses with the same soluble/insoluble ratio had roughly the same values, ranging from 0.910 to 0.918. However, the S65.5 (lowest S/I ratio) had the highest ratio with a value of 0.938, while the S51.0 (highest S/I ratio) had the lowest value, at 0.883. Additionally, it can be noted from Figure 2 that the mean ring value in gels decreases almost linearly (R^2=0.941) with the Si % content, which is equivalent to the (B+Al) content.

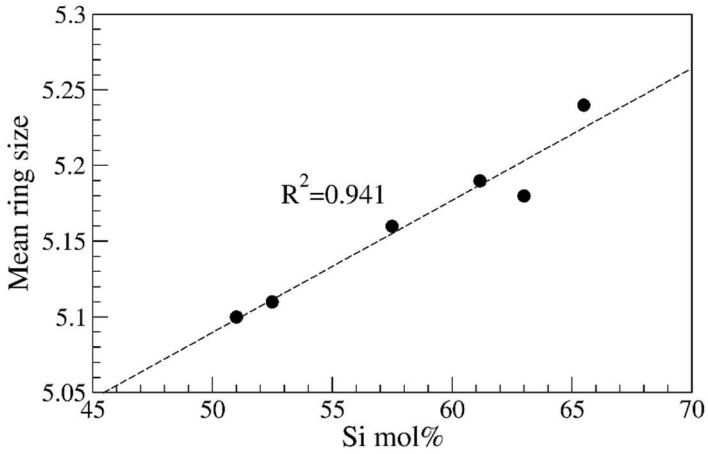

Figure 2 – Evolution of the mean ring size of the gel with Si content (mol%) in the initial glass

Pore size distribution

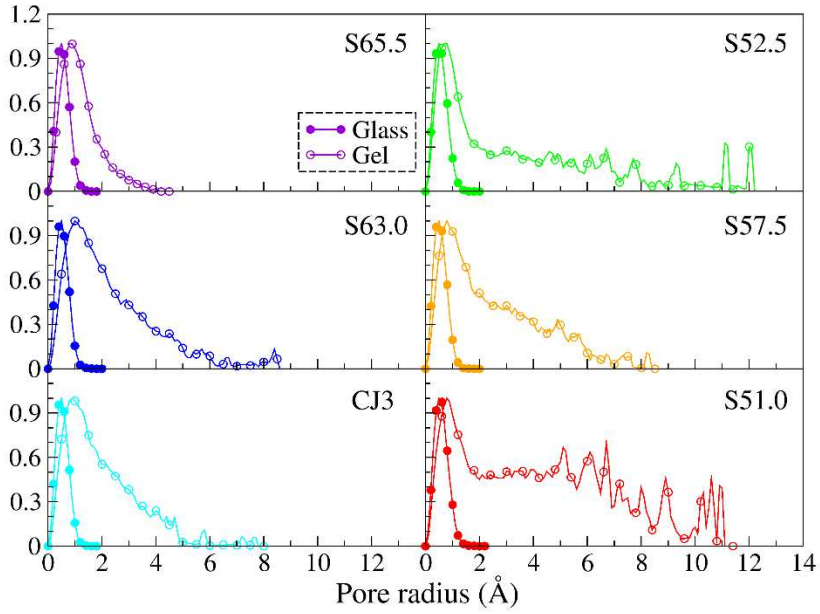

Figure 3 – Pore size distribution in the initial glasses and in the dry gels

The pore size distribution (PSD) was calculated for the dry gels and the initial glasses as a reference for the free volume intrinsic to the glasses, using the method of Bhattachary and Gubbins[43]. Hereafter are considered as 'pores' only the volume that enables the transport of an H_2O molecule, thus pores with a radius larger 1.25 Å, which correspond to the maximum free volume visible in the glasses. These results are presented in Figure 3. It can be seen that for all the glasses, the PSD is roughly the same, with a maximum of distribution at around 0.5 Å which slightly increases with a decrease in density. However, the shapes of the PSD differ significantly between the gels. The pore radius is at its maximum for the gels prepared from the glasses with the highest B content, and then decreases as the B content in the glasses decreases.

Structural factors

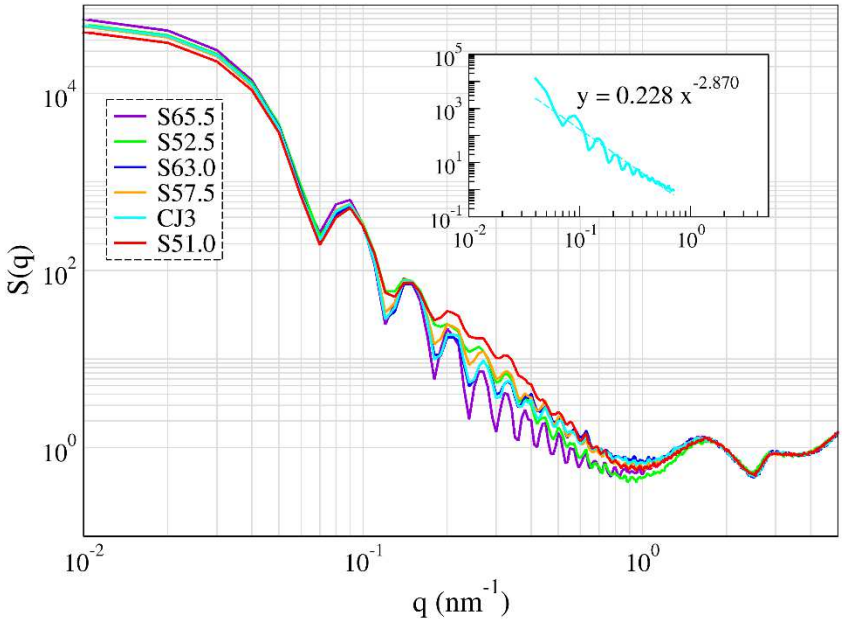

Figure 4 –Structural factors S(q) of the simulated alteration gels

	S65.5	S63.0	CJ3	S52.5	S57.5	S51.0
n	3.165	2.824	2.870	3.169	2.906	2.853

Table 5 – Exponent n extracted from a fit of the structure factors by the power law q^{-n} in the dry gels

The structure factors *S*(*q*) derived from the calculated SAXS spectra were obtained following the same method as that used by Cailleteau et al.[14]. The results are presented in Figure 4. While the shape of the curve fluctuates considerably (certainly induced by the relatively small size of the system), the exponent *n* can be calculated from the power law q^{-n} regression in order to evaluate the regularity of the pores. Between 1 and 3 the exponent is indicative of the pore structure, whereas between 3 and 4 it is representative of the surface of the pores. In fact, an increase in the pore regularity corresponds to an increase in the exponent from 3 to 4.The exponent values for the dry gels can be found in Table 5. As they remain relatively close (2.82 to 3.17) despite the wide composition range, it seems to have little effect on the pore regularity.

Structural evolution of the “dry” gels during the annealing at 2400 K

Coordination number

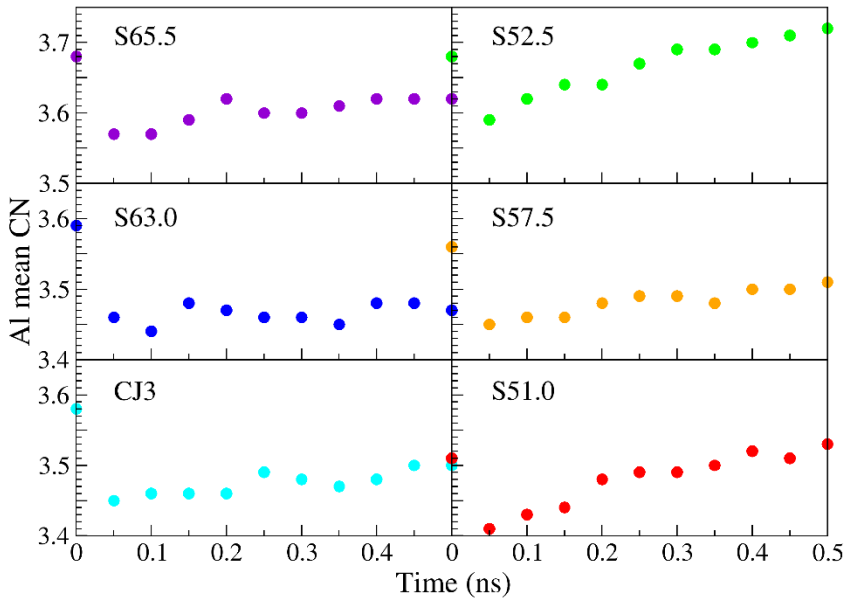

Figure 5 – Aluminium CN in the dry gels versus time during the annealing at 2400 K

Figure 5 and Figure 6 display the time dependency of the mean Al CN and Ca CN, respectively, during the 0.5 ns annealing stage at 2400 K. For all the gels, a major decrease can be observed immediately after the beginning of the annealing relaxation due to the thermal motions (the temperature was raised from 300K to 2400K for the annealing). The coordination numbers in the gel structures equilibrated at 300K are given in Table 4, but this section shows how the dynamics of dry gel formation occur during the annealing stage at 2400K.

Hereafter, a reconstruction of the Al^4 and Ca environments occurs, with its efficiency depending on the gel. From these results, two behaviours can be deduced: gels for which the reorganisation is only slight (S65.5, S63.0, CJ3), and gels for which the reorganisation is more developed (S52.5, S57.5, S51.0).

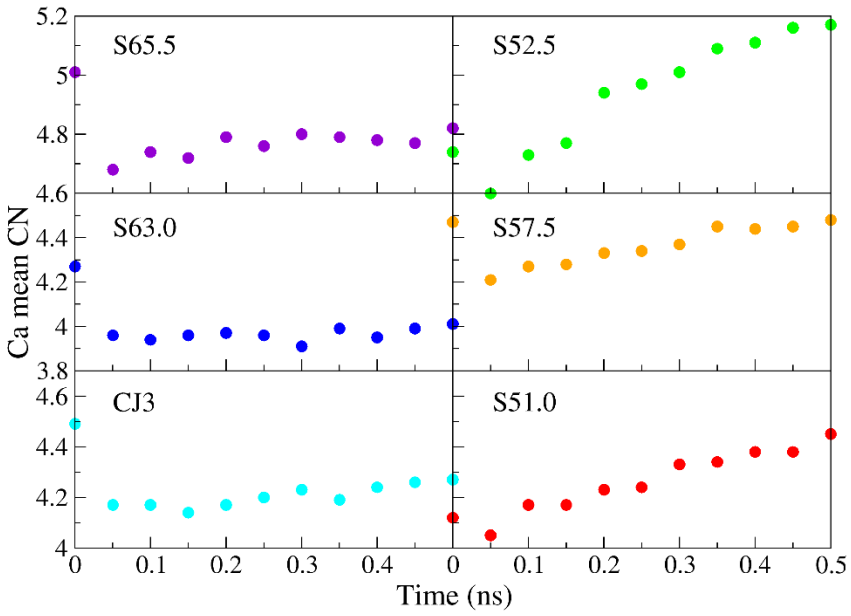

Figure 6 – Calcium CN in the dry gels versus time during the annealing at 2400 K

NBO and O^3

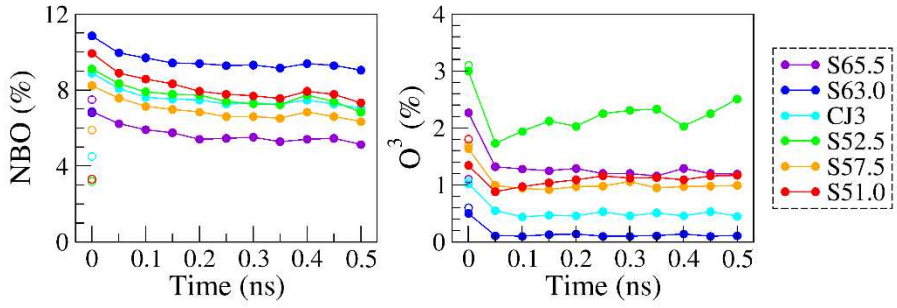

Figure 7 – NBO and O^3 percentages evolution of the dry gels versus time during the annealing at 2400 K. Empty symbols represent the NBO and O^3 percentages in the initial glasses.

Figure 7 displays the evolution of the NBO and O^3 percentages through the annealing at 2400K. One can see through the comparison between the NBO percentage in the initial glass and at the beginning of the annealing, that the removal of the B and Na induces a significant increase of NBO percentage (except for S65.5, which shows a slight decrease). The NBO percentage then decreases by roughly 2 % during the annealing and is stabilised quite quickly after around 0.2 ns. The comparison between the O^3 percentage in the initial glass and at the beginning of the annealing displays few modifications (except for S65.5, which shows an increase and S51.0, which shows a decrease). During the annealing at 2400K, the O^3 percentage is stabilised rapidly at 0.05 ns. It can be noted that the O^3 % increases with the Al % in the glass, confirming what has been shown previously in the glass and in the final gel (see Table 4).

During annealing at 2400K, the NBO percentage decreases and the O^3 percentage increases. It means that there is a global increase of the polymerization level of the structures. A correlation between the Al coordination change (Figure 5) and the polymerization level change can be noted. The polymerization level change has been estimated by calculating the quantity $\%O^3$ - %NBO (Figure 8). Globally, the larger the increase of the polymerisation level, the larger the increase of the Al coordination during annealing.

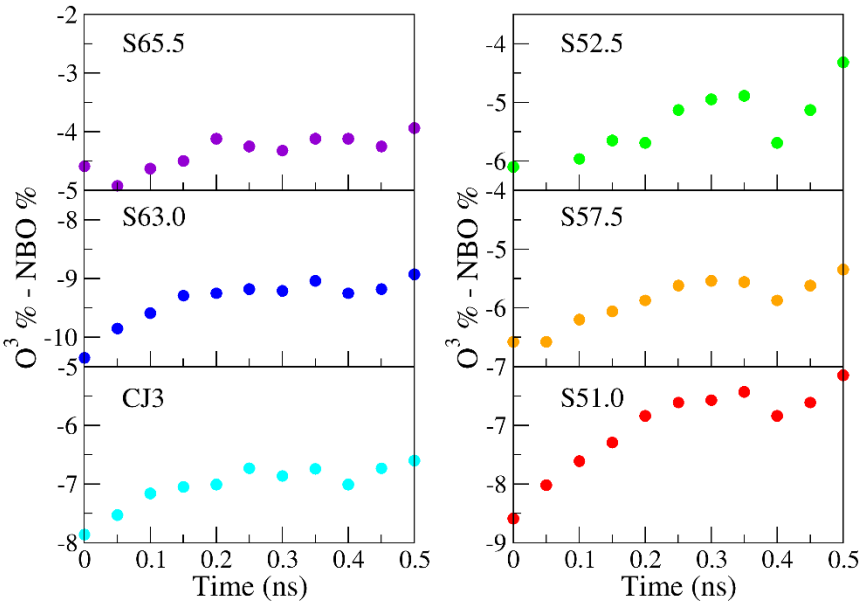

Figure 8 – Evolution of O3% - NBO% of the dry gels versus time during the annealing at 2400 K

Rings

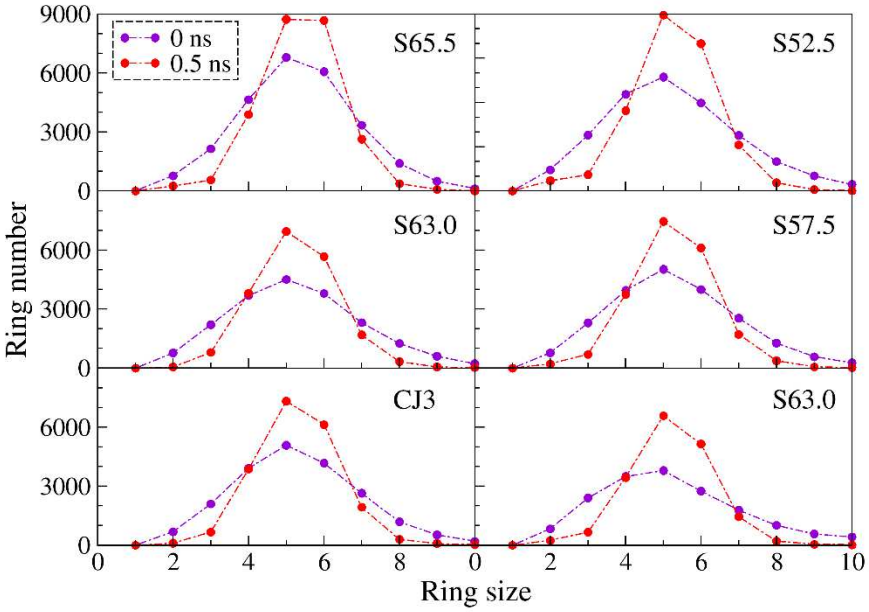

Figure 9 – King ring size distributions in the dry gels before and after the annealing at 2400 K

The King ring size distribution just before and immediately after the annealing are compared in Figure 9. The presence of 2-membered rings at the beginning of the annealing but no longer visible at the end is coherent with the observation of few Si-O-Si, O-Si-O, and Si-O-Al angles equal to 90° (not shown here). All distributions are centred on 5-membered rings. A narrowing of the distribution is observed for the six gels after annealing. A characteristic "reorganisation" time τ, corresponding to the reconstruction of the network at 2400 K, can be estimated by fitting the FWHM (Full Width Half Maximum) change with time during the annealing as $FWHM = A + Be^{-t/\tau}$. From these values, displayed in Table 6, it seems that a lower Si content is associated with a longer relaxation time, which can probably be ascribed to a more flexible network (the S65.5 structure is an exception). However, this correlation remains weak.

	S65.5	S63.0	CJ3	S52.5	S57.5	S51.0
τ (ns)	0.0620	0.0479	0.0467	0.0592	0.0606	0.0560

Table 6 – Characteristic "reorganisation" time τ estimated from the narrowing versus time of the King ring size distribution of the gels during the annealing at 2400 K

Pore size distribution

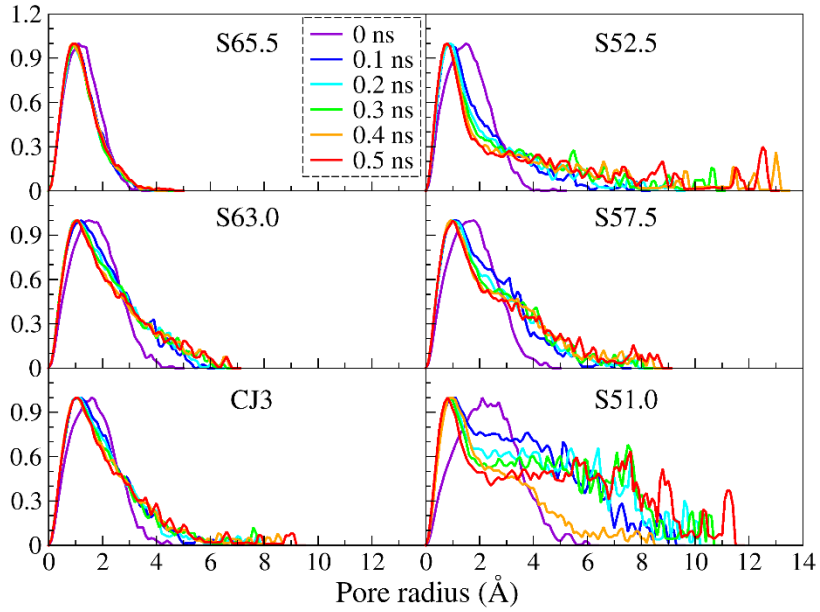

Figure 10 – PSD evolution of the dry gels versus time during the annealing at 2400 K

From the PSD evolution versus time illustrated in Figure 10, the formation of pores with greater radii can be observed for all the gels, but the increase in progressive distribution spreading strongly depends on the composition. For S57.5, S52.5, and S51.0, a larger and faster spreading of the distributions can be observed compared to CJ3, S63.0, and S65.5. The ratio of the final compared to the initial mean pore radius has been calculated from values displayed in Supplementary Information Figure S2 and evolves as S52.5 > S51.0 > S57.5 > CJ3 > S63.0 > S65.5. This confirms the two behaviours previously identified. The gels formed from glasses with a lower Si content (S52.5, S51.0, S57.5) present a more developed reorganisation than the gels formed from glasses with a higher Si content (S65.5, S63.0, CJ3).

Surface atoms

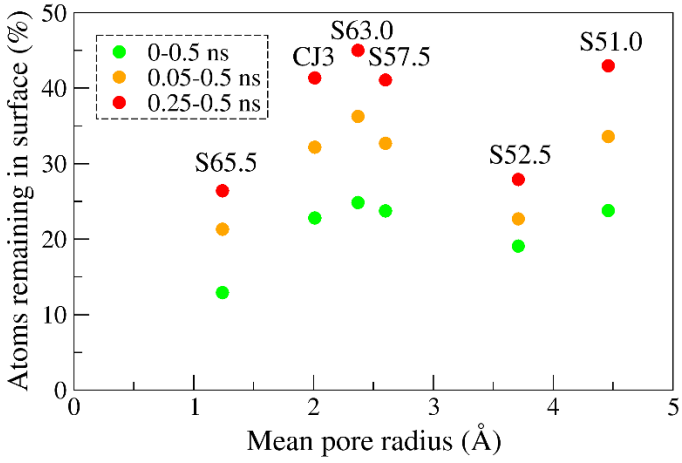

Figure 11 – Evolution of the percentage of atoms remaining at the pore surfaces during different time intervals of the annealing versus the mean pore radius of the gels

The number of atoms on the pore surfaces was calculated for all the gels. Their evolution through time can be found in the Supplementary Information Figure S3. It appears that the number of surface atoms mainly increased at the beginning of the annealing for most of the gels, then remained fairly constant (or decreased slightly for S52.5). Also, the number of surface atoms is directly linked to the number of atoms removed initially, as shown in Supplementary Information Figure S4.

However, even if the number of surface atoms remained roughly constant, it appears (Figure 11) that only ≈20% of the atoms initially present on the surface at the beginning of the annealing were still on the pore surfaces at its end. This is indicative of a fast reorganisation during the annealing. It is nevertheless greater at the beginning of the relaxation, as between 0.05 and 0.5 ns at least 30% of the atoms remained on the pore surfaces for most of gels. Additionally, during the second half of the relaxation nearly 40% of the surface atoms were stabilised on the pore surfaces, which is indicative of a slowing down of the gel reorganisation. No clear trend between the number of surface atoms and the pore size is recognisable.

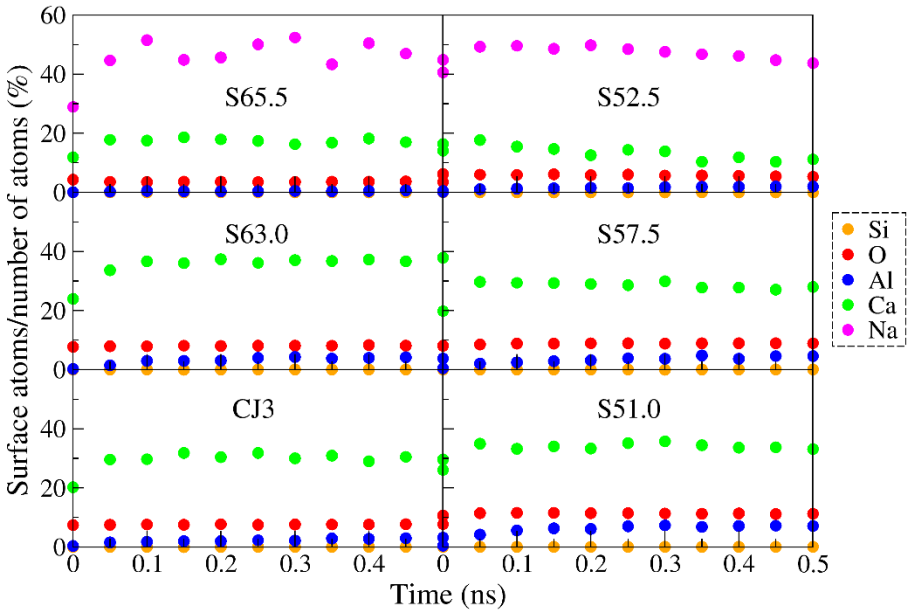

Figure 12 - Evolution of the percentage of atoms on the pore surfaces (relatively to the total number of atoms in the system) versus time for the different atom species

The surface atom types were investigated (see Supplementary Information Figure S5). It appears that some atom types are more likely to be at the pore surfaces. For all gels, the O atoms were predominant and they represented roughly 80% of all the pore surface atoms. Then followed Na (for S52.5), Ca with ≈15%, Al within the 1-4% range, and finally Si with less than 0.2%. Furthermore, when normalised to the total quantity of atoms of a given type, it seems from Figure 12 that mobile elements such as Na and Ca can be found in a higher proportion at the pore surface compared to O, Al, and Si. It should be noted that at least 50% of Na atoms were present on the pore surfaces for the two Na-containing gels. For these, 20% of the calcium atoms were surface atoms whereas on the Na-depleted gels, their proportion increased to reach values between 30 to 40%. It is interesting to see that Na-containing gels carry just enough Na to compensate all the Al. However, if 50% of them are

on the pore surfaces, they are no longer available for charge-compensation. This could partially explain the high number of 3-fold coordinated Al in the gels.

Atomic displacements

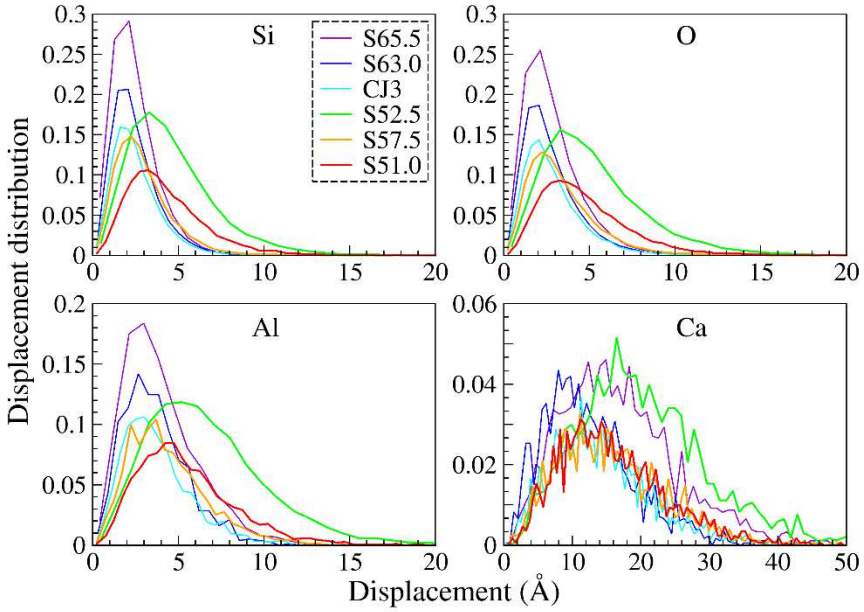

Figure 13 – Displacement distributions of Si, O, Al, and Ca during the dry gel annealing at 2400 K.

Figure 13 shows the atomic displacement distribution of the six gels for Si, O, Al, and Ca. The mean values of these distributions are presented in Supplementary Information Figure S6. From these Figures it can be seen that the mobility of the different types of atoms increased as Si < O < Al < Ca. The higher mobility of aluminium compared to oxygen is unexpected, as the opposite is generally documented when diffusion is calculated at different temperatures in equilibrated glasses. Moreover, the mobility of the atoms depends on the gel composition. The atomic displacements in the S52.5, S51.0, and S57.5 gels were greater than in the S63.0, S52.5, and S65.5 gels (except for the Ca in S65.5). The atomic displacements represent further evidence that the gels formed from glasses with a lower Si content reorganise more during the annealing at 2400K.

	τ_{Si} (ns)	τ_{O} (ns)	τ_{Al} (ns)	τ_{Ca} (ns)
S65.5	0.065	0.068	0.081	0.162
S63.0	0.059	0.060	0.067	0.117
CJ3	0.062	0.065	0.069	0.132
S52.5	0.135	0.129	0.133	0.149
S57.5	0.073	0.075	0.087	0.134
S51.0	0.087	0.086	0.094	0.137

Table 7 – "Reorganisation time" τ calculated from the average displacement versus time for Si, O, Al, and Ca in the simulated gels during the annealing relaxation at 2400 K

In Table 7 can be found the characteristic "reorganisation" time τ associated with the Si, O, Al, and Ca displacements. These values were calculated by fitting the average displacements per atom type

versus time with $\bar{S}(t) = A(1 - e^{-t/\tau})$. For each gel, comparison of τ per atom type reflects the same trend as previously seen, following Si < O < Al < Ca. The higher the "reorganisation" time of an atom type, the longer it moves. The Ca showed the greatest mobility, probably due to its network modifier role, and was therefore less impacted by the polymerised network. Also, when comparing the different gels, it can be seen that the characteristic "reorganisation" time for all the atom types evolved as S52.5 > S51.0 > S57.5 > S65.5 > CJ3 > S63.0 (except for the Ca in S65.5, which was higher than all the other gels), confirming the two possible behaviours of a gel depending on the Si content in the initial glass.

Discussion

Structural changes between the initial glass and the dry gel

Local order

Some local order structural differences can be pointed out between the glasses and their gels. The removal of all boron atoms seemed to trigger the formation of a more polymerised silicon network for the majority of the gels, with the increase of Si Q_4 species at the expense of Q_3. While this trend has been suggested by NMR experimental results obtained by Collin et al. on the ISG[10], it was also noted that the decrease of the chemical shift for Si could be the result of a second-neighbour effect and not come from a higher polymerisation degree. In the case described here, the overall increase in Q_4 species could be the result of a surface effect, as a large proportion of the network modifiers were present on the surface of the pores and thus not available to form NBOs. This effect may disappear in further simulation when water is added, creating silanol groups at the pore surface. However, the opposite phenomenon was observed for the S51.0 and S52.5 gels, for which a decrease of Si Q4 species of around 4% was observed. These gels were prepared from the glasses with the lowest silicon content, respectively 51% and 52.5% (and also the highest boron content). This decrease may originate from the high number of charges to be compensated in the original glasses, thus limiting the number of NBOs, which then increases in the gels. Conversely, the largest change in the Q_n population occurred for the S65.5, which was the glass with the highest (63%) silicon content. Between the S65.5 glass and its gel, Si Q_4 species increased by 10%. Therefore, the least destabilised glasses seem to lead to a more reticulated gel network. It can also be noted that NBOs were more often found attached to silicon atoms rather than aluminium atoms. Allwardt et al.[48] had already observed this experimentally. As stated earlier, an increase in the number of tricoordinate oxygens can be observed in the gels compared to the glasses. This suggests that the stabilisation of some four-fold coordinated aluminium in the gels is achieved by O^3 entities[49], even if the theoretical total number of charges would enable a full compensation of aluminium atoms.

Effect of the initial perturbation induced by the removal of B and Na

The most apparent effect of the initial perturbation, namely the removal of B and Na, can be observed on the pore size of the gels. The mean pore size as well as the global pore size distribution increased with an increasing boron content in the initial glass, as seen in Figure 3. Across the compositional range studied, the mean pore radius values range from 1.25 Å up to 4.5 Å. Additionally, the variations in composition lead to different maximal pore radii, up to 12 Å for S52.5. Considering the wide range of pore sizes obtained from the various compositions, it seems appropriate to evaluate the impact of both the size and surfaces of the pores on the structure of the surrounding gel network.

Several variations in coordination as well as in bond angles are attributed to surface effects, meaning their relatively higher occurrence at the surface of pores. The increase of three-fold coordinated aluminium as well as the decrease in calcium coordination number can be indicative of such effects. As can be seen in Figure 14, the 3-fold coordinated Al appears to be mostly present at the surface of the pores compared to the 4-fold coordinated Al. Moreover, the study of the surface atoms indicates that, on average, 97% of the Al on the pore surfaces are 3-fold coordinated. The decrease in the coordination number could also be ascribed to the global depletion in oxygen atoms, necessary to maintain charge neutrality in the gels (see Methods), which is intrinsically linked to the pore surface. Furthermore, a large proportion of the charge compensators were found on the pore surface, thus not available for charge compensation in the gel network. It can also be noted that the increase in three-fold coordinated aluminium seems to be larger when the aluminium content decreases through the series. However, this could be the result of statistical effects as no clear correlation can be determined.

As a result, a slight increase (up to nearly two degrees) in the mean O-Al-O angle was observed, which is consistent with an increasing population of Al^3 tending to reach a 120° trihedral angle. Additionally, Si-O-Si and Si-O-Al mean angle values decreased in the gels compared to the glasses, which is consistent with observations reported elsewhere[35,36] and attributed to surface effects. However, when compared to Rimsza et al.[36], the decrease appears to be much smaller: around 1-2° here, compared to approximately 9° in their work. In order to better understand the origin of this effect, it is necessary to study the dynamics of gel formation.

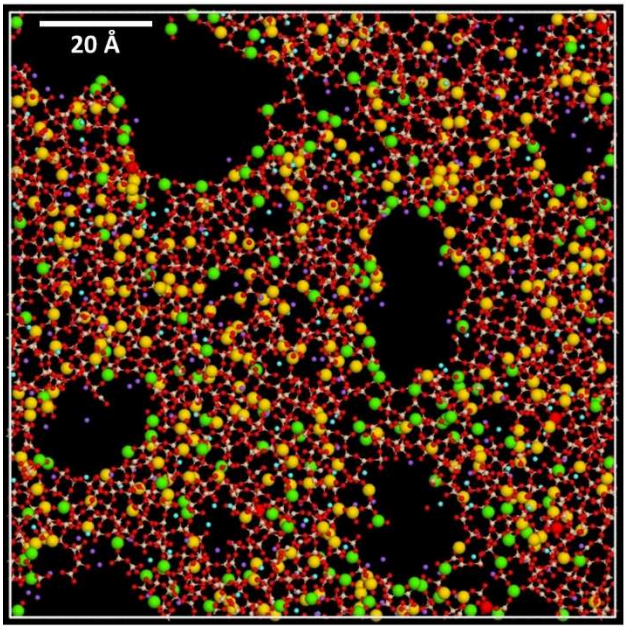

Figure 14 – View of a slice of the S52.5 gel. Large atoms are 3-fold coordinated Al atoms in green, 4-fold coordinated in yellow, and 5 fold-coordinated in red. Small spheres represent: in beige, Si atoms; in red, oxygen atoms; in purple, Na atoms; and in cyan, calcium atoms.

The dynamics of the gel reorganisation points to two distinct behaviours that seem to originate from the initial degree of destabilisation undergone by the materials after the removal of B and Na. The displacement distributions for the different species give the first insights into the reorganisation within the gels. It can be seen that while calcium atoms were the most mobile cations during the reorganisation, aluminium atoms came just after them. This may be because highly distorted aluminium sites lead to a greater relaxation. In equilibrated glasses, it has been generally observed that the Al atoms displace less than the O atoms. The contrary was observed here, probably because

of the large initial perturbation associated with the B and Na removals. As a consequence, Al atoms needed to displace more to rebuild their stable environments.

Additionally, two behaviours were clearly seen among the gels, with S65.5, S63.0, and CJ3 showing the lowest displacements for all atom types, as opposed to S52.5, S51.0, and S57.5, which showed the highest mobility and thus a greater reorganisation. Several other features at different range orders support this result. On the intermediate range order, it appears from the PSD (Figure 10) and the mean pore size (Supplementary Information) that the evolution of the pore sizes within the gels depends on the gel composition. Pore size exhibits a larger increase for the gels (S52.5, S51.0, S57.5) formed from the glasses with lower Si % content, and alternatively greater (B+Al) % content. The highly disrupted shape of the PSD for these gels suggests that there might be more interconnected pores than in the gels formed from glasses presenting a larger Si % content[32].

On the short-range order, the evolution of the mean CN for both Al and Ca during the reorganisation process validated the existence of two categories of gels with distinct relaxation degrees. Again, S52.5, S51.0, and S57.5 showed a greater increase of these CN and thus a better reconstruction of the local environments around these atoms compared to the S65.5, S63.0, and CJ3 gels. Furthermore, when comparing the evolution of the Al and Ca mean CN with the mean pore radius during the reorganisation of the different gels, the two distinct behaviours appear even more clearly. Figures 15 and 16 display the Al CN and Ca CN, respectively, as a function of the mean pore radius during the annealing at 2400K. In the three gels S52.5, S57.5, and S51.0, a linear evolution of the Al and Ca CN with the mean pore size can be observed. This result is a supplementary indication that two types of behaviours can be identified, with S52.5, S57.5, and S51.0 corresponding to the gels that present the largest and longest reorganisation, as opposed to S65.5, S63.0, and CJ3 which show only slight signs of reorganisation. This can be linked to the initial destabilisation of the gels. Furthermore, for the S52.5, S57.5, and S51.0 gels, the slopes in Figures 15 and 16 are the same for Al on one part and Ca on the other part (3 times higher for Ca than for Al). This could indicate that one elementary change in one Al or one Ca local environment is associated with the same variation of the pore volume, irrespective of the gel composition.

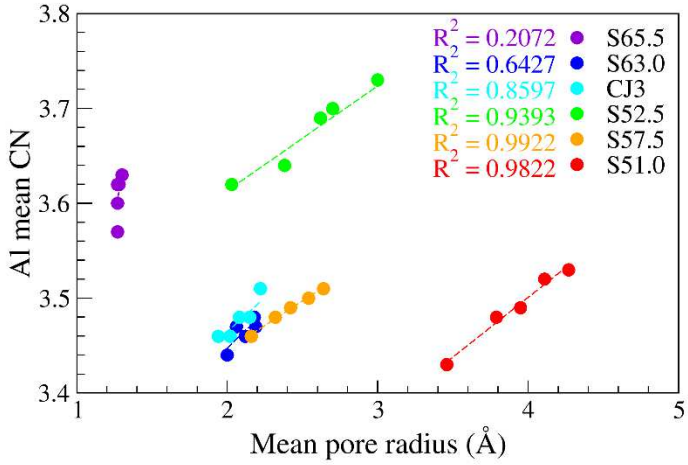

Figure 15 – Aluminium CN evolution versus the mean pore size in the dry gels during the annealing at 2400 K

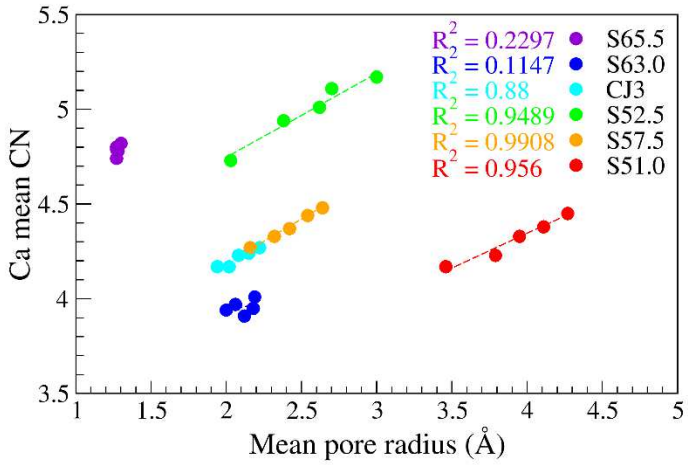

Figure 16 – Calcium CN evolution versus the mean pore size in the dry gels during the annealing at 2400 K

Comparison with literature

The results we obtained can be considered to be at an interface between earlier work performed by Rimsza and Du on "dry" silica gels[36], and work on gels formed from multicomponent glasses[32] using different methods.

The first comparison is made with a recent work performed on hydrated gel structures[32] using the REAXFF method. The gels were obtained with two different methods: introduction of a hydrogarnet defect on dense silica and removal of three different percentages of Si atoms, and soluble species removal from a simplified international simple glass (sISG). In the study presented here, water was not present. Comparison between dry and hydrated materials should provide insights into the mechanisms by which gels form and evolve. Furthermore, the gels studied here contained Si, Al, Ca, and some contained Na, while in Rimsza and Du's work, the gels were formed from pure silica. Also, our systems are two orders of magnitude larger. Similar results were nevertheless obtained for the ring size distributions, with values centred on five-membered rings. It should be noted that for our glasses, the ring size centred around six-membered rings, which differs from what was obtained for the sISG (centred around five) and which is comparable to CJ3 (with 5.81% of Ca substituted for Na_2O). Another difference resides in the number of Si Q_n species, as we found between 81% and 91% Q_4 in both glasses and gels with the rest being mainly Q_3, while there was only a rather small percentage of Q_4 in their system (around 10%). However, both methods present some degrees of repolymerisation between the simulated glass and the gel, with an increase in Q_4 at the expense of Q_3 in our case, and an increase of Q_3 and Q_4 at the expense of Q_2 and Q_1 in their case. This difference could be explained by the fact that there was no water in our systems, or because the Q4 percentage was initially higher in our CJ3 glass. Finally, the PSD we obtained do not have the same or similar shapes as those they obtained. This might primarily be due to a larger system which enabled bigger pores to form in our study samples. However the S65.5 gel, despite its larger size, was the only one that displayed a similar shape. Nevertheless considering the differences in compositions, no clear correlation can be found.

It is also interesting to compare the work described here with Rimsza and Du's work on dry gels[36]. The dry gels they studied were silica gels obtained using two different methods called volume scaling (VS), for which the cell volume size is linearly increased from dense amorphous silica, and charge

scaling (CS), which consists in simulating nanoporous silica by increasing the ionic charge for each simulation step. For both methods they observed an increase in structural defects, mainly the presence of three-fold coordinated Si with increasing porosity. It is interesting to note that in the absence of other elements, defects appeared on Si (up to 6% Si^3 with the VS method), while in our study the Si remained tetra coordinated and the defects concentrated around the Al local environments. This confirms the high stability of the SiO_4 tetrahedron compared to the AlO_4 tetrahedron. When comparing the angle distributions, in Rimsza and Du's study the formation of a small shoulder at 90° can be seen, indicative of the presence of two-membered rings, mainly near the surface of the pores. This was also clearly visible in our gels. However, the shoulder disappeared after relaxation because the two-membered rings are easily annealed. It can also be observed that the maximum of the Si-O-Si bond angle distribution decreases when using the VS method, due to both a variation in density as well as surface effects. This was however not observed with the CS method. It thus appears that our method is closer to the VS method, which is more representative of a chemical vapour deposition (CVD) process in terms of pore morphology, than to the CS (more like sol-gel processing).

Conclusion

To sum up, this study focussed on dry gels obtained from alumino-borosilicate glasses with varying soluble/insoluble and SiO_2/Al_2O_3 ratios in order to investigate the impact of glass compositions on gel properties. A new method is proposed, consisting in removing the B and Na atoms from the glass and annealing the resulting structure at high temperature.

We analysed primarily the pore size and morphology. As expected, the mean pore radius increased with increasing boron content in the glass, but interestingly various maximal pore sizes were found which could be indicative of interconnected pores. Most of the structural defects were found on Al, and lead to an increase in three-fold coordinated aluminium, especially at the pore surfaces. This surface effect was confirmed by a decrease in the Si-O-Si and Si-O-Al mean angles.

The study of the reorganisation dynamics of the different gels highlighted two distinct behaviours which did not correspond to the hypotheses emitted when designing the compositions. The gels formed from the glasses with the largest Si content displayed the lowest displacements for all the atomic species, as well as the smallest pore sizes and recovery of the Al and Ca local environments, as opposed to the gels formed from the glasses with lower Si content. This is indicative of a larger and longer reorganisation of the gels when the initial perturbation is higher. Interestingly, it was shown that while Ca is the most mobile cation, it was closely followed by Al, which was not expected as Al mobility is usually less than that of O in equilibrated glasses. It is thus suggested that both their displacements are interdependent to some extent, and considerable reorganisations occur around the Al and Ca atoms during the gel reorganisation. This has also been pointed out by the linear evolution of both Al and Ca mean CN with the mean pore radius for the gels that reorganize the most.

Finally, the comparison with works performed by Rimsza and Du[32,36] enabled us to find qualitatively similar results, with the decreased ring size in certain gels compared to glasses, as well as defects concentrated at the pore surfaces. The next step is to add water to our systems, in order to fully characterize more realistic gels. This may well have effects on the gel structures and pore surfaces.

Acknowledgement

This work was supported as part of the Center for Performance and Design of Nuclear Waste Forms and Containers, an Energy Frontier Research Center funded by the U.S. Department of Energy, Office of Science, Basic Energy Sciences under Award # DE-SC0016584. The authors are grateful to Jincheng Du and his team (University North Texas) for the work done on the potentials development.

References

1 Morse, D. L. & Evenson, J. W. Welcome to the Glass Age. *Int J Appl Glass Sci* **7**, 409-412, doi:10.1111/ijag.12242 (2016).

2 Gin, S. *et al.* An international initiative on long-term behavior of high-level nuclear waste glass. *Mater Today* **16**, 243-248, doi:10.1016/j.mattod.2013.06.008 (2013).

3 Vienna, J. D., Ryan, J. V., Gin, S. & Inagaki, Y. Current Understanding and Remaining Challenges in Modeling Long-Term Degradation of Borosilicate Nuclear Waste Glasses. *Int J Appl Glass Sci* **4**, 283-294, doi:10.1111/ijag.12050 (2013).

4 Donald, I. W. *Waste immobilization in glass and ceramic based hosts: radioactive, toxic and hazardous wastes*. (John Wiley & Sons, 2010).

5 Grambow, B. Nuclear waste glasses - How durable? *Elements* **2**, 357-364, doi:DOI 10.2113/gselements.2.6.357 (2006).

6 Gin, S. *et al.* Nuclear Glass Durability: New Insight into Alteration Layer Properties. *J Phys Chem C* **115**, 18696-18706, doi:10.1021/jp205477q (2011).

7 Frankel, G. S. *et al.* A comparative review of the aqueous corrosion of glasses, crystalline ceramics, and metals. *npj Materials Degradation* **2**, 15, doi:10.1038/s41529-018-0037-2 (2018).

8 Gin, S. *et al.* Origin and consequences of silicate glass passivation by surface layers. *Nat Commun* **6**, doi:Artn 6360

10.1038/Ncomms7360 (2015).

9 Rebiscoul, D. *et al.* Morphological evolution of alteration layers formed during nuclear glass alteration: new evidence of a gel as a diffusive barrier. *J Nucl Mater* **326**, 9-18, doi:10.1016/j.jnucmat.2003.10.015 (2004).

10 Collin, M. *et al.* Structure of International Simple Glass and properties of passivating layer formed in circumneutral pH conditions. *npj Materials Degradation* **2**, 4, doi:10.1038/s41529-017-0025-y (2018).

11 Munier, I., Crovisier, J. L., Grambow, B., Fritz, B. & Clement, A. Modelling the alteration gel composition of simplified borosilicate glasses by precipitation of an ideal solid solution in equilibrium with the leachant. *J Nucl Mater* **324**, 97-115, doi:10.1016/j.jnucmat.2003.08.033 (2004).

12 Hellmann, R. *et al.* Unifying natural and laboratory chemical weathering with interfacial dissolution–reprecipitation: a study based on the nanometer-scale chemistry of fluid–silicate interfaces. *Chem Geol* **294**, 203-216 (2012).

13 Gin, S. *et al.* Dynamics of self-reorganization explains passivation of silicate glasses. *Nat Commun* **9**, doi:Artn 2169

10.1038/S41467-018-04511-2 (2018).

14 Cailleteau, C., Devreux, F., Spalla, O., Angeli, F. & Gin, S. Why Do Certain Glasses with a High Dissolution Rate Undergo a Low Degree of Corrosion? *J Phys Chem C* **115**, 5846-5855, doi:10.1021/jp111458f (2011).

15 Du, T. *et al.* Atomistic origin of the passivation effect in hydrated silicate glasses. *npj Materials Degradation* **3**, 6, doi:10.1038/s41529-019-0070-9 (2019).

16 Gin, S., Beaudoux, X., Angeli, F., Jegou, C. & Godon, N. Effect of composition on the short-term and long-term dissolution rates of ten borosilicate glasses of increasing complexity from 3 to 30 oxides. *J Non-Cryst Solids* **358**, 2559-2570, doi:10.1016/j.jnoncrysol.2012.05.024 (2012).
17 Fournier, M. *et al.* Effect of pH on the stability of passivating gel layers formed on International Simple Glass. *J Nucl Mater* **524**, 21-38, doi:10.1016/j.jnucmat.2019.06.029 (2019).
18 Arena, H. *et al.* Impact of Zn, Mg, Ni and Co elements on glass alteration: Additive effects. *J Nucl Mater* **470**, 55-67, doi:10.1016/j.jnucmat.2015.11.050 (2016).
19 Guo, X. L. *et al.* Self-accelerated corrosion of nuclear waste forms at material interfaces. *Nat Mater* **19**, 310-+, doi:10.1038/s41563-019-0579-x (2020).
20 Collin, M., Fournier, M., Charpentier, T., Moskura, M. & Gin, S. Impact of alkali on the passivation of silicate glass. *npj Materials Degradation* **2**, 16, doi:10.1038/s41529-018-0036-3 (2018).
21 Chave, T., Frugier, P., Gin, S. & Ayral, A. Glass-water interphase reactivity with calcium rich solutions. *Geochim Cosmochim Ac* **75**, 4125-4139, doi:10.1016/j.gca.2011.05.005 (2011).
22 Mercado-Depierre, S., Angeli, F., Frizon, F. & Gin, S. Antagonist effects of calcium on borosilicate glass alteration. *J Nucl Mater* **441**, 402-410, doi:10.1016/j.jnucmat.2013.06.023 (2013).
23 Tribet, M. *et al.* New Insights about the Importance of the Alteration Layer/Glass Interface. *J Phys Chem C* **124**, 10032-10044, doi:10.1021/acs.jpcc.0c02121 (2020).
24 Reiser, J. T. *et al.* Comparative structural investigations of nuclear waste glass alteration layers and sol-gel synthesized aerogels. *npj Materials Degradation* **4**, 5, doi:10.1038/s41529-020-0109-y (2020).
25 Kerisit, S., Pierce, E. M. & Ryan, J. V. Monte Carlo simulations of coupled diffusion and surface reactions during the aqueous corrosion of borosilicate glasses. *J Non-Cryst Solids* **408**, 142-149, doi:10.1016/j.jnoncrysol.2014.07.020 (2015).
26 Hopf, J. *et al.* Glass-water interaction: Effect of high-valence cations on glass structure and chemical durability. *Geochim Cosmochim Ac* **181**, 54-71, doi:10.1016/j.gca.2016.02.023 (2016).
27 Gin, S. *et al.* A General Mechanism for Gel Layer Formation on Borosilicate Glass under Aqueous Corrosion. *J Phys Chem C* **124**, 5132-5144, doi:10.1021/acs.jpcc.9b10491 (2020).
28 Du, J. in *Molecular Dynamics Simulations of Disordered Materials: From Network Glasses to Phase-Change Memory Alloys* (eds Carlo Massobrio, Jincheng Du, Marco Bernasconi, & Philip S. Salmon) 157-180 (Springer International Publishing, 2015).
29 Deng, L. & Du, J. C. Development of effective empirical potentials for molecular dynamics simulations of the structures and properties of boroaluminosilicate glasses. *J Non-Cryst Solids* **453**, 177-194, doi:10.1016/j.jnoncrysol.2016.09.021 (2016).
30 Ha, M.-T. & Garofalini, S. H. Local structure of network modifier to network former ions in soda-lime alumino-borosilicate glasses. *J Am Ceram Soc* **100**, 563-573, doi:10.1111/jace.14565 (2017).
31 Ohkubo, T., Gin, S., Collin, M. & Iwadate, Y. Molecular Dynamics Simulation of Water Confinement in Disordered Aluminosilicate Subnanopores. *Sci Rep-Uk* **8**, doi:Artn 3761
10.1038/S41598-018-22015-3 (2018).
32 Rimsza, J. M. & Du, J. Nanoporous silica gel structures and evolution from reactive force field-based molecular dynamics simulations. *npj Materials Degradation* **2**, 18, doi:10.1038/s41529-018-0039-0 (2018).
33 Collin, M. *et al.* Molecular Dynamics Simulations of Water Structure and Diffusion in a 1 nm Diameter Silica Nanopore as a Function of Surface Charge and Alkali Metal Counterion Identity. *J Phys Chem C* **122**, 17764-17776, doi:10.1021/acs.jpcc.8b03902 (2018).

34 Miyoshi, H., Hata, N. & Kikkawa, T. Theoretical Investigation into Effects of Pore Size and Pore Position Distributions on Dielectric Constant and Elastic Modulus of Two-Dimensional Periodic Porous Silica Films. *Japanese Journal of Applied Physics* **44**, 1166-1168, doi:10.1143/jjap.44.1166 (2005).
35 Beckers, J. V. L. & de Leeuw, S. W. Molecular dynamics simulation of nanoporous silica. *J Non-Cryst Solids* **261**, 87-100, doi:Doi 10.1016/S0022-3093(99)00607-9 (2000).
36 Rimsza, J. M. & Du, J. C. Structural and Mechanical Properties of Nanoporous Silica. *J Am Ceram Soc* **97**, 772-781, doi:10.1111/jace.12707 (2014).
37 Nakano, A., Bi, L. S., Kalia, R. K. & Vashishta, P. Molecular-Dynamics Study of the Structural Correlation of Porous Silica with Use of a Parallel Computer. *Phys Rev B* **49**, 9441-9452, doi:DOI 10.1103/PhysRevB.49.9441 (1994).
38 Angeli, F., Gaillard, M., Jollivet, P. & Charpentier, T. Influence of glass composition and alteration solution on leached silicate glass structure: A solid-state NMR investigation. *Geochim Cosmochim Ac* **70**, 2577-2590, doi:10.1016/j.gca.2006.02.023 (2006).
39 Fluegel, A. Global model for calculating room-temperature glass density from the composition. *J Am Ceram Soc* **90**, 2622-2625, doi:10.1111/j.1551-2916.2007.01751.x (2007).
40 Jégou, C. *Mise en évidence expérimentale des mécanismes limitant l'altération du verre R7T7 en milieu aqueux. Critique et proposition d'évolution du formalisme cinétique*, (1998).
41 Plimpton, S. Fast Parallel Algorithms for Short-Range Molecular-Dynamics. *J Comput Phys* **117**, 1-19, doi:DOI 10.1006/jcph.1995.1039 (1995).
42 Le Roux, S. & Jund, P. Ring statistics analysis of topological networks: New approach and application to amorphous GeS2 and SiO2 systems. *Comp Mater Sci* **49**, 70-83, doi:10.1016/j.commatsci.2010.04.023 (2010).
43 Bhattacharya, S. & Gubbins, K. E. Fast method for computing pore size distributions of model materials. *Langmuir* **22**, 7726-7731, doi:10.1021/la052651k (2006).
44 Pedone, A. Recent Advances in Solid-State NMR Computational Spectroscopy: The Case of Alumino-Silicate Glasses. *Int J Quantum Chem* **116**, 1520-1531, doi:10.1002/qua.25134 (2016).
45 Atila, A., Ghardi, E., Hasnaoui, A. & Ouaskit, S. Alumina effect on the structure and properties of calcium aluminosilicate in the percalcic region: A molecular dynamics investigation. *J Non-Cryst Solids* **525**, doi:ARTN 119470
10.1016/j.jnoncrysol.2019.119470 (2019).
46 Bouhadja, M., Jakse, N. & Pasturel, A. Striking role of non-bridging oxygen on glass transition temperature of calcium aluminosilicate glass-formers. *J Chem Phys* **140**, doi:Artn 234507
10.1063/1.4882283 (2014).
47 Benoit, M., Ispas, S. & Tuckerman, M. E. Structural properties of molten silicates from ab initio molecular-dynamics simulations: Comparison between CaO-Al2O3-SiO2 and SiO2. *Phys Rev B* **64**, doi:Artn 224205
10.1103/Physrevb.64.224205 (2001).
48 Allwardt, J. R., Lee, S. K. & Stebbins, J. F. Bonding preferences of non-bridging O atoms: Evidence from O-17 MAS and 3QMAS NMR on calcium aluminate and low-silica Ca-aluminosilicate glasses. *Am Mineral* **88**, 949-954, doi:Doi 10.2138/Am-2003-0701 (2003).
49 Delaye, J.-M. *et al.* Investigation of alumino-silicate glasses by coupling experiments and simulations: Part I - Structures. *Manuscript submitted for publication* (2020).